ELSEVIER

Journal of Nuclear Materials 306 (2002) 121–125

journal of nuclear materials

www.elsevier.com/locate/jnucmat

Effects of Xe-ion irradiation at high temperature on single crystal rutile

Fuxin Li [a,b], Ping Lu [a], K.E. Sickafus [b,*]

[a] Department of Materials Science and Engineering, New Mexico Institute of Mining and Technology, Socorro, NM 87801, USA
[b] Materials Science and Technology Division, Los Alamos National Laboratory, MS-G755, Los Alamos, NM 87545, USA

Received 21 March 2002; accepted 7 September 2002

Abstract

Rutile (TiO_2) single crystals with (1 1 0) orientation were irradiated with 360 keV Xe^{2+} ions at 923 K to fluences ranging from 7×10^{14} to 1×10^{16} Xe/cm^2. Damage accumulation and evolution were analyzed using Rutherford backscattering spectroscopy combined with ion channeling analysis, and cross-sectional transmission electron microscopy. TiO_2 crystals were found to exhibit a layer-like damage structure after irradiation, with up to three characteristic layers: (1) a thin surface layer denuded of defects; (2) a second layer centered at the peak damage position, consisting of small voids about 1–3 nm in diameter; and (3) a third, deeper layer consisting of large defects such as dislocations and dislocation loops. The defect-denuded layer at the surface results from point defect diffusion and annealing. The voids in the second layer may be attributed to aggregation of vacancies. Point defect migration and precipitation is also responsible for the large defects observed in the deepest layer within the irradiated microstructure. Amorphization was not observed in the crystals irradiated at this high temperature.

1. Introduction

Rutile (TiO_2) is a semiconductor widely used in electrical and optical applications. Ion irradiation offers the possibility to modify the physical and optical properties of materials such as rutile. Several investigations on radiation damage effects in rutile have been reported [1–9]. These studies examined radiation effects for irradiation temperatures ranging from about 7 K to room temperature (300 K). No studies, however, have been reported on radiation effects at higher temperatures. Due to recovery processes, the radiation response of rutile at high temperature is expected to be different from that at lower temperature. Two major differences are anticipated. The amorphization process, which occurs readily at relatively low temperatures, is usually suppressed at elevated temperature, due to enhanced mobility and a corresponding high recovery efficiency for point defects. On the other hand, void swelling, which seldom occurs at relatively low temperatures, becomes more probable at elevated temperature due to the high mobility of vacancies. In this paper, we report on radiation effects in TiO_2 single crystals irradiated at 923 K with 360 keV Xe^{2+} ions. Damage microstructures were studied by combining Rutherford backscattering spectrometry and ion channeling (RBS/C) with cross-sectional transmission electron microscopy (XTEM).

2. Experimental

Single crystals of rutile (TiO_2) with (1 1 0) orientation were obtained from Princeton Scientific (P.O. Box 143, Princeton, NJ 08542) for use in this study. The wafers were polished on one side to a mirror finish and cut to

* Corresponding author. Tel.: +1-505 665 3457; fax: +1-505 667 6802.
E-mail address: kurt@lanl.gov (K.E. Sickafus).

0022-3115/02/$ - see front matter
PII: S0022-3115(02)01234-5

dimensions of about $10 \times 10 \times 0.5$ mm^3. Ion irradiation experiments were performed using a 200 kV ion implanter in the Ion Beam Materials Laboratory at Los Alamos National Laboratory. The implanter was operated at 180 kV in order to obtain 360 keV Xe^{2+} for irradiation. Samples were attached firmly to a metal stage heated to 923 K and tilted about 15° with respect to the beam axis during irradiation to avoid channeling effects. The temperature of the stage was monitored with a thermocouple during irradiation. Three samples were irradiated sequentially in one operation. Samples were irradiated to fluences of 7×10^{14}, 2×10^{15}, and 1×10^{16} Xe/cm^2, while maintaining a constant ion flux of about 2.5×10^{12} Xe/cm^2 s (this flux is similar to that used in previous experiments [8,9]). After irradiation, samples were cooled to room temperature in about 1 h.

Ion irradiated samples were analyzed first using RBS/C along a $\langle 1\,1\,0 \rangle$ crystallographic axis using a 2 MeV He^+ ion beam. Samples were then prepared in cross-section for examination by transmission electron microscopy (TEM). The radiation-induced microstructure was examined in a Philips CM 30 microscope operating at 300 keV.

Fig. 1 shows the projected range of the implanted Xe (solid-line) and the corresponding displacement damage (dashed-line) profile. These profiles were estimated using the Monte Carlo simulation program SRIM [10]. A threshold displacement energy of 40 eV was used for both Ti and O elements in these calculations (this choice is arbitrary). The longitudinal range of 360 keV Xe-ions in rutile (15° from normal incidence) is about 80 nm with a longitudinal straggling of about 24 nm. The peak radiation dose for the highest ion fluence used in these experiments (1×10^{16} Xe/cm^2) is approximately 29 displacements per atom (dpa). This maximum occurs at a depth of ≈60 nm. This peak is also approximately four times the dpa level at the sample surface. The peak Xe concentration at the maximum Xe-ion fluence is about 1.6 at.% Xe. This concentration is centered at a sample depth of about 80 nm.

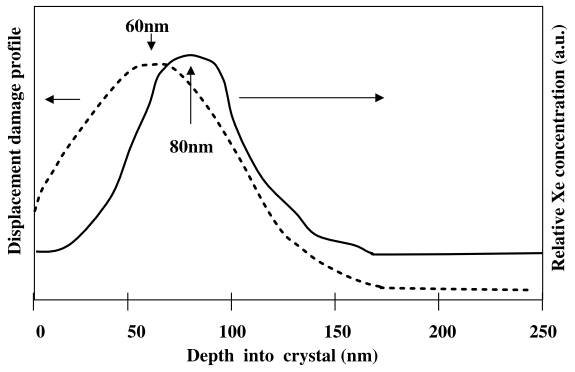

Fig. 1. Displacement damage (- - -) and Xe-ion concentration (—) profiles for 360 keV Xe-ion implantation into rutile (TiO_2), based on calculations using the Monte Carlo simulation program SRIM-2000.

3. Results and discussion

Fig. 2 shows RBS/C spectra obtained from three $(1\,1\,0)$ TiO_2 single crystals irradiated to different fluences at 923 K. The aligned spectra were obtained using a 2 MeV He^+ ion beam aligned along the $\langle 1\,1\,0 \rangle$ TiO_2 crystallographic axis. For comparison, an aligned spectrum and a random spectrum from an unirradiated sample are also shown in Fig. 2. The aligned spectra for the high temperature irradiated samples are quite different from those obtained from TiO_2 crystals irradiated at room temperature [8,9]. First, examining the RBS high-energy edge corresponding to scattering from surface Ti atoms (1.43 MeV in Fig. 2), a defect-denuded layer appears in the spectral region corresponding to Ti atoms near the sample surface, whereas in the case of room temperature irradiated samples, a surface damage peak was observed at this position. Second, the RBS/C damage peaks, which appear at a depth near the mean Xe-ion projected range (behind the high-energy Ti edge at about 1.35 MeV), are rather broad compared to the damage peaks observed for room temperature irradiated TiO_2. Third, even for the sample irradiated to the highest fluence (1×10^{16} Xe/cm^2), the observed Ti damage peak in the RBS/C spectrum (Fig. 2) is still considerably below that of the random spectrum. This

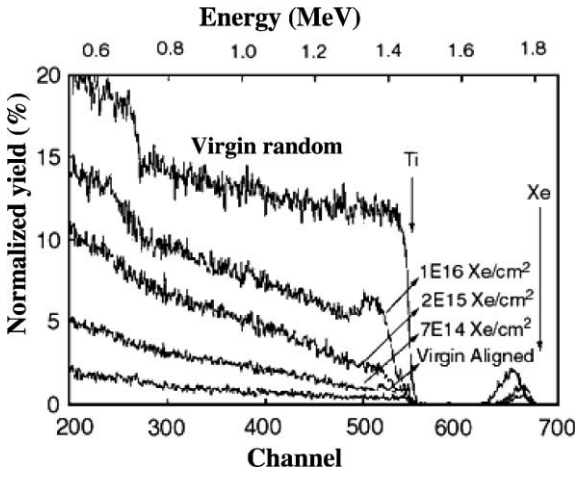

Fig. 2. 2 MeV He^+ ion RBS/C spectra obtained from $(1\,1\,0)$-oriented TiO_2 single crystals irradiated with 360 keV Xe^{2+} at 920 K to increasing ion fluence. A random and an aligned spectrum from an unirradiated crystal are also shown for comparison.

indicates that no amorphous layer was formed under high temperature irradiation. By contrast, under room temperature irradiation conditions, an amorphous layer was observed at a fluence of about 7×10^{15} Xe/cm^2 [8].

According to the Rutherford backscattering/channeling spectrometry theory [11], the backscattering yield at depth x in an aligned spectrum consists of two components. These are shown schematically in Fig. 3. Component 1 is primarily the result of backscattering from interstitial-type point defects, while component 2 is due to dechanneling of the incident beam induced by lattice strain. Based on the aligned RBS/C spectrum obtained at the highest Xe-ion fluence (1×10^{16} Xe/cm^2 in Fig. 2), component 2 appears significantly larger than component 1. This indicates that after the high temperature irradiation, the interstitial concentration in the crystals is relatively small while the lattice supports a significant amount of strain. The lattice strain could result from defects such as dislocations and voids. Using methods described elsewhere, the concentration of displaced atoms from an aligned RBS/C spectrum can be quantified [11]. If this concentration is compared to the number of instantaneously produced point defects based on SRIM, then the survivability of point defects can be estimated. The ratio of surviving to instantaneous point defects (interstitials) on the Ti sublattice at the highest Xe-ion fluence (1×10^{16} Xe/cm^2) and at a depth corresponding to the peak damage, is about 1.5%. This ratio for room temperature irradiations was about 4.2% at the same ion fluence [12].

The irradiated samples used for RBS/C analysis were prepared in cross-section for TEM analyses, in order to determine the nature and distribution of defects. Fig. 4(a)–(c) show bright-field (BF) TEM micrographs obtained from TiO_2 crystals irradiated to fluences of (a) 7×10^{14}; (b) 2×10^{15}; and (c) 1×10^{16} Xe/cm^2, respectively. BF images in Fig. 4(a) and (b) were obtained with the electron beam aligned along $\vec{B} = [0\,0\,1]$, while the BF image in Fig. 4(c) was obtained with the electron beam aligned along $\vec{B} = [1\,\bar{1}\,0]$.

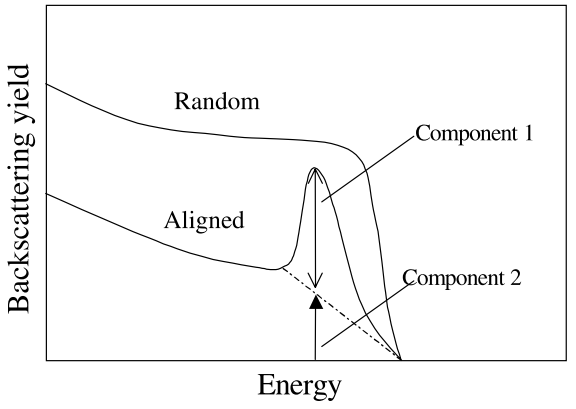

Fig. 3. Partitioning of the He^+ ion backscattering yield into two components for a hypothetical aligned RBS/C spectrum from a crystal containing radiation damage. Component 1 results from backscattering from interstitial-type point defects, while component 2 is due to dechanneling of the incident beam induced by lattice strain.

For the crystal irradiated to fluence 7×10^{14} Xe/cm^2, no damage microstructure is visible within the irradiated region (Fig. 4(a)). When the fluence is increased to 2×10^{15} Xe/cm^2 (Fig. 4(b)), defects become visible in the irradiated region. The damage microstructure consists of two layers: a defect-denuded layer at the surface with a thickness of about 40 nm, followed by a damage layer with thickness of about 60 nm, in which two sets of dislocations are visible. Using $\vec{g} \cdot \vec{b}$ analysis [13], the Burgers vectors of the dislocations were determined. The two sets of the dislocations visible in Fig. 4(b) have projected line directions parallel to [1 0 0] and [0 1 0] directions and have Burgers vectors consistent with $\vec{b} = [1\,0\,0]$ or $[0\,1\,0]$ (the edge or screw character of the dislocations was not determined in this study).

For the crystal irradiated to fluence 1×10^{16} Xe/cm^2 (Fig. 4(c)), three damage layers are apparent in the irradiated region. The total thickness of the irradiated region at this fluence is about 200 nm. The top layer (1) is a defect-denuded layer with thickness of about 25 nm. Immediately beneath this layer is a second layer (2) with a thickness of about 45 nm, which is characterized by small voids about 1–3 nm in diameter. The third layer (3) with a thickness of about 130 nm contains dislocations whose character is similar to those observed at lower fluence (Fig. 4(b)).

The microstructural features in Fig. 4(c) with an appearance like that of voids, could arise due to aggregation of vacancies or from precipitation of implanted Xe atoms. In the latter case, the void-like objects are actually Xe bubbles. In order to understand the reasons for void or bubble formation, the implanted Xe profile for the high temperature, high-dose Xe-ion irradiated rutile sample based on RBS/C measurements (Fig. 2), was compared to the TEM damage microstructure (Fig. 4(c)). Fig. 5 shows a comparison between the measured RBS/C Xe profile (solid curve) and a cross-sectional TEM micrograph showing the void distribution in the 1×10^{16} Xe/cm^2 irradiated rutile. For comparison, the Xe-ion profile for 360 keV ion-irradiated rutile, calculated using SRIM, is also shown in Fig. 5 (dotted-line). The measured and calculated Xe-ion profiles in Fig. 5 are almost identical, indicating that the redistribution of Xe after high temperature irradiation is negligible. The void-like features in Fig. 5 are located at depths ranging from approximately 30–70 nm, while the peak Xe concentration (measured and calculated) peak resides at a depth of about 80 nm. The position of the void-like band is, on average, about 30 nm shallower than the Xe

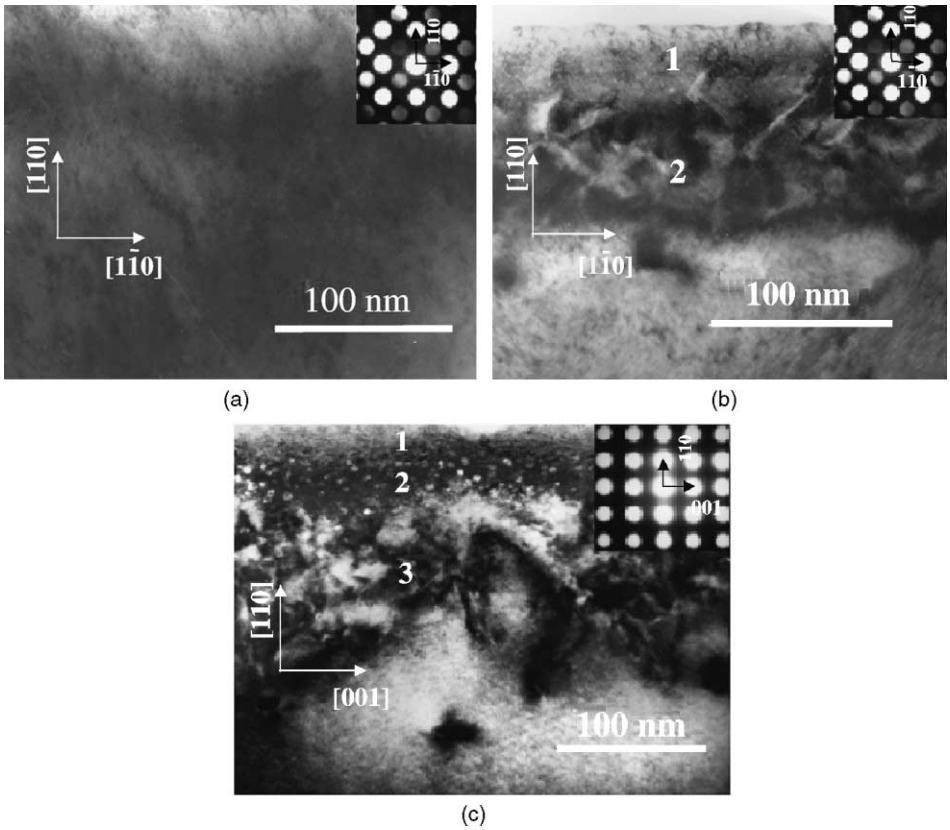

Fig. 4. Cross-sectional TEM micrographs obtained from (1 1 0)-oriented rutile crystals irradiated at 920 K to fluences of (a) 7×10^{14}; (b) 2×10^{15}; and (c) 1×10^{16} Xe/cm^2, respectively. Microdiffraction patterns from the irradiated regions are also shown as insets.

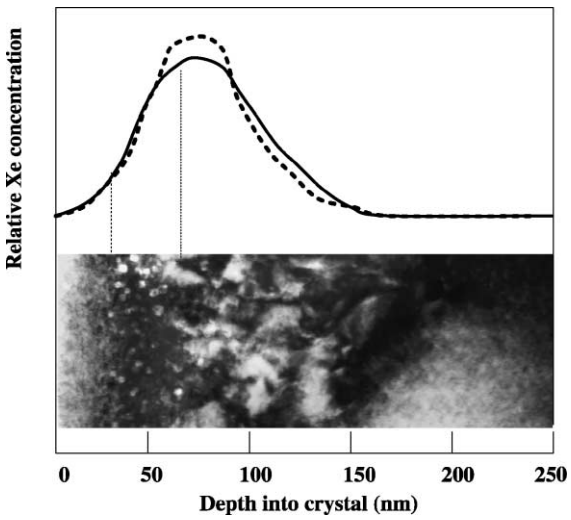

Fig. 5. XTEM micrograph obtained from a (1 1 0) TiO_2 crystal irradiated to a fluence of 1×10^{16} Xe/cm^2 at 920 K. Also shown are the measured Xe-ion profile based on RBS/C (solid curve) and the calculated Xe-ion profile (···) based on SRIM results for the same ion fluence. The vertical dotted-lines indicate the approximate positions of the void-like band.

peak position and is in better coincidence with the peak of the ion damage profile (Fig. 1). Based on these considerations, it is likely that the void-like features visible in TEM images are a direct result of the aggregation of vacancies produced by ballistic damage events.

The observed microstructures in Fig. 4(b) and (c) may be rationalized considering the diffusion properties of point defects produced under irradiation. Both interstitials and vacancies produced near the sample surface can diffuse outward and annihilate at the free surface (i.e., the surface acts as a point defect sink). The defect-denuded layers evident in Fig. 4(b) and (c) are due to this effect. Denuded zones can occur near surfaces (or other point defect sinks such as grain boundaries) because point defect concentrations are reduced to near thermal equilibrium values, and therefore dislocation loop (or void) nucleation and growth rates are suppressed [14]. Similar microstructures have been observed in radiation damage studies on many ceramics, such as cubic zirconia (ZrO_2) [15] and quartz (SiO_2) [16]. Interstitials produced at depths well below the surface are more likely to be absorbed at the perimeters of growing interstitial-type clusters and dislocation loops. Vacancies produced well below the surface will participate in void

growth, provided their mobilities are sufficiently large. The microstructures observed in Fig. 4(b) and (c) suggest certain qualitative features regarding the relative mobilities of interstitials and vacancies in high temperature irradiated TiO_2. The fact that voids are not observed until high ion dose while dislocations are observed at moderate dose suggests that, for the irradiation and temperature conditions used in this study, interstitials on either sublattice (cation and anion) have significantly higher mobilities than vacancies. Also, since the voids observed at high-dose are confined to the vicinity of the peak in the damage profile (25–70 nm, Fig. 1), while the dislocations at this dose extend to depths far from the peak damage region, the inference again is that interstitials are more mobile than vacancies.

4. Conclusion

Radiation damage effects in rutile single crystals irradiated with 360 keV Xe^{2+} ions at 923 K has been studied combining RBS/C analyses with cross-sectional TEM. The results can be summarized as follows:

(1) At this high temperature, no amorphization transformation is observed, even at a fluence of 1×10^{16} Xe/cm^2. This is due in part to the small survivability ($\sim$1.5%) of the point defects produced by irradiation.
(2) For crystals irradiated to low fluence (7×10^{14} Xe/cm^2), the retained defect concentration is so low that no damage microstructure is resolved by TEM.
(3) After irradiated to a medium fluence (for example 2×10^{15} Xe/cm^2), the damage structure consists of a defect-denuded layer followed by a layer with dislocations. The defect-denuded layer forms because point defects have sufficient mobility to diffuse and annihilate in the vicinity of the free surface. The deeper damage layer with dislocations presumably results from cation and anion interstitial aggregation and growth.
(4) As the fluence is increased to the highest level used in this study (1×10^{16} Xe/cm^2), the damage microstructure consists of three layers. The top layer is again a defect-denuded layer. The middle layer consists of small voids about 1–3 nm in diameter. This layer results from condensation of vacancies. The third, deepest layer is a layer containing dislocations, as was observed in the microstructure at lower dose.

Acknowledgements

We are grateful to Caleb Evans and Mark Hollander at Los Alamos National Laboratory for their help with Xe-ion irradiations in the Los Alamos Ion Beam Materials Laboratory. This research was sponsored by the US Department of Energy, Office of Basic Energy Sciences, Division of Materials Sciences.

References

[1] R. Fromknecht, O. Meyer, Mater. Chem. Phys. 45 (1996) 50.
[2] R. Fromknecht, R. Auer, I. Khubeis, O. Meyer, Nucl. Instrum. and Meth. B 120 (1996) 252.
[3] I. Khubeis, O. Meyer, Nucl. Instrum. and Meth. B 120 (1996) 257.
[4] I. Khubeis, R. Fromknecht, O. Meyer, Phys. Rev. 55 (1) (1997) 136.
[5] O. Meyer, I. Khubeis, R. Fromknecht, S. Massing, Nucl. Instrum. and Meth. B 127&128 (1997) 624.
[6] O. Meyer, I. Khubeis, R. Fromknecht, S. Massing, Nucl. Instrum. and Meth. B 136–138 (1998) 436.
[7] I. Khubeis, R. Fromknecht, S. Massing, O. Meyer, Nucl. Instrum. and Meth. B 141 (1998) 332.
[8] F. Li, P. Lu, K. Sickafus, Mater. Res. Symp. Proc. 540 (1999) 311.
[9] F. Li, M. Ishimaru, P. Lu, K.E. Sickafus, Philos. Mag. B 80 (2000) 1947.
[10] J.F. Ziegler, J.P. Biersack, U. Littmark, The Stopping Range of Ions In Solids, Pergamon, New York, 1985.
[11] W.-K. Chu, J.W. Mayer, M.-A. Nicolet, Backscattering Spectrometry, Academic, New York, 1978, Chapter 8.
[12] F. Li, M. Ishimaru, P. Lu, I.V. Afanasyev-Charkin, K.E. Sickafus, Nucl. Instrum. and Meth. B 166&167 (2000) 314.
[13] D.B. Williams, C.B. Carter, Transmission Electron Microscopy, Plenum, New York, 1996, Chapter 25.
[14] S.J. Zinkle, in: R.E. Stoller, A.S. Kumar, D.S. Gelles (Eds.), Effects of Radiation on Materials: 15th International Symposium, ASTM STP, vol. 1125, American Society for Testing and Materials, Philadelphia, 1992, p. 749.
[15] N. Yu, K.E. Sickafus, P. Kodali, M. Nastasi, J. Nucl. Mater. 244 (1997) 266.
[16] W.L. Gong, L.M. Wang, R.C. Ewing, J. Zhang, Phys. Rev. B 54 (1996) 3800.